Lattice dynamical study and the interpretation of the phase transitions in tetrafluoroaluminate $RbAlF_4$

1989 J. Phys.: Condens. Matter 1 9301

(http://iopscience.iop.org/0953-8984/1/47/003)

J. Phys.: Condens. Matter 1 (1989) 9301–9312. Printed in the UK

Lattice dynamical study and the interpretation of the phase transitions in tetrafluoroaluminate $RbAlF_4$

G L Hua
Department of Physics, Monash University, Clayton, Victoria, Australia

Received 17 July 1989

Abstract. A comprehensive study into the symmetry and normal vibrations of tetrafluoroaluminates $RbAlF_4$ along Γ–Δ–X–Y–M–V–A in the Brillouin zone for both phases I and II is conducted by using the multiplier representation of the group theory. The consistency of the symmetry and the phonon mode patterns along M–V–A (the [001] direction), and the anisotropy of the compatibility relations along the [001] axis and along the [100] and [010] axes are further evidence for the characteristic layer structure of $RbAlF_4$. The non-ferroic first-order structural phase transition (SPT) at $T_{c1} = 553$ K, which is induced by the condensation of the phonon mode τ_3, and the ferroelastic second order SPT at $T_{c2} = 282$ K, which is the result of the softening of the complex conjugate modes τ_1 and τ_7, are interpreted by the lattice vibration modes derived from our study. The interpretation of these successive displacive phase transitions is in good agreement with result from the experimental investigation.

1. Introduction

The structure of the layered perovskites $A^IM^{III}F_4$ is built up by MF_6 octahedra linked together in a two-dimensional array in the (001) plane and disconnected along the [001] axis (figure 1). In the highest-symmetry phase (aristotype structure), the MF_6 octahedra are centred in a tetragonal cell with the A^+ cations at the corner (Brosset 1937). Successive structural phase transitions have been observed in these materials and they have attracted great interest in recent years. In particular, the tetrafluoroaluminates $AAlF_4$, such as $RbAlF_4$, $TlAlF_4$, $KAlF_4$, undergo several displacive phase transitions stimulated by the tilting of the octahedra AlF_6 (Bulou *et al* 1983). Experimental investigation showed that these successive tilts of the relative rigid octahedra could be interpreted by the condensation of soft phonon modes at M $(\frac{1}{2}\,\frac{1}{2}\,0)$, X $(0\,\frac{1}{2}\,0)$ or A $(\frac{1}{2}\,\frac{1}{2}\,\frac{1}{2})$ points in the Brillouin zone of the ideal aristotype structure (Bulou *et al* 1983). The tilting motion of the rigid octahedra AlF_6 appears to be the deciding factor not only for the understanding of the phase transitions in layered perovskite $A^IM^{III}F_4$, but also to the understanding of the phase transitions in other perovskites in which the MF_6 octahedra are linked together in a three-dimensional network. Studies of these successive phase transitions could provide new information into the problems of the displacive or order–disorder character of ferroelastic phase transitions (Rousseau 1979). They could also provide additional information for the general theory of phase transitions.

$RbAlF_4$ undergoes two successive structural phase transitions, one at $T_{c1} = 553$ K (first-order SPT, non-ferroic) and another at $T_{c2} = 282$ K (second-order SPT, ferroelastic). They have been studied by DSC, x-ray and neutron diffraction (Bulou and Nouet

0953-8984/89/479301+12$02.50

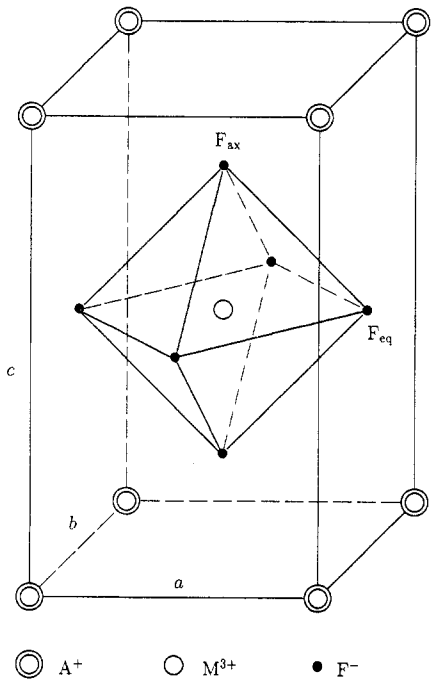

Figure 1. Aristotype structure of the tetrafluoroaluminate $RbAlF_4$.

1982) and by birefringence (Kleemann *et al* 1982). At high temperature, $RbAlF_4$ phase I has the aristotype structure with space group P4/mmm (D^1_{4h}). Below T_{c1} in phase II, the octahedra tilt around the [001] axis and the new unit cell volume is doubled, with the new axes making an angle of 45° to the phase I unit cell. Phase II is tetragonal too, with spacegroup P4/mbm (D^5_{4h}). Below T_{c2} in phase III, the AlF_6 octahedra undergo two new tilts around the [100] and [010] axes, and the rubidium (Rb) ions shift along the [001] axis at the same time. The unit cell volume is again doubled in the (001) plane. This phase is orthorhombic with space group Pmmn (D^{13}_{2h}). These unit cells of the successive structures are shown in figure 2. Crystal dynamical investigations into $RbAlF_4$, including an infrared study of the aristotype structure (Soga *et al* 1974), a Raman scattering study of the SPT at T_{c1} and at T_{c2}, and a lattice dynamical calculation of the phonon spectrum based on a rigid-ion model (Bulou *et al* 1983, 1987) are reported in the literature. In this paper we present a comprehensive study into the symmetry and normal vibrations of $RbAlF_4$ for both phases I and II by the multiplier representation of the group theory (Maradudin and Vosko 1968) and a lattice dynamical interpretation of the successive displacive structural phase transitions in the tetrafluoroaluminate $RbAlF_4$.

2. Symmetry and the normal vibrations in phase I and II

The symmetry properties and the symmetry vibration modes of $RbAlF_4$ in phase I and II are obtained by using the multiplier representation of the group theory (Maradudin and Vosko 1968). The Kovalev symmetry notations (Kovalev 1965) used in our nomenclature are compared with the notations from Bulou *et al* (1983)

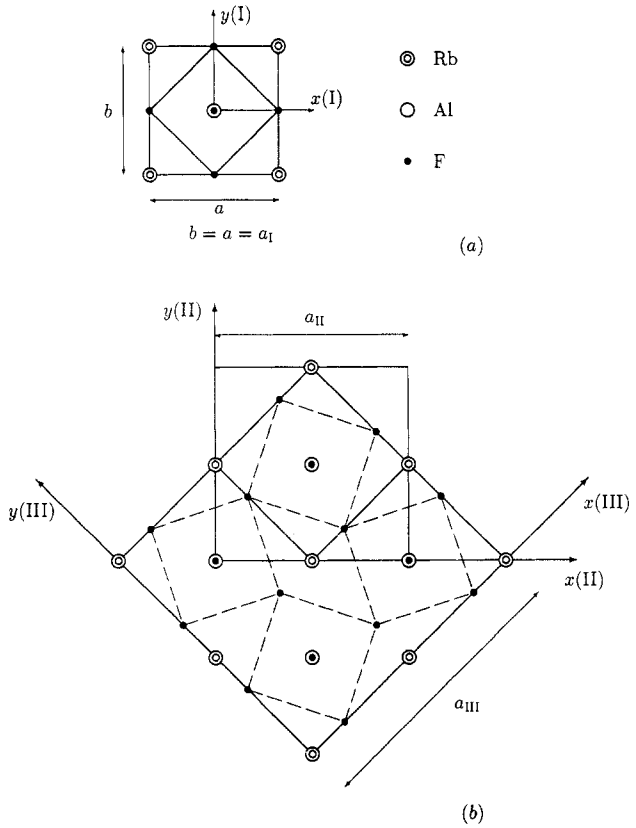

Figure 2. The unit cell projections on the (001) plane of $RbAlF_4$ in (*a*) phase I and (*b*) phase II and III.

where necessary. The symmetry properties of phase I, along Γ–Δ–X–Y–M–V–A, and the symmetry properties of phase II, along Γ–Δ–X–Y–M, in the Brillouin zone are presented in tables 1 and 2. The compatibility relations along these directions are given in figure 3. The condition for compatibility of representations along a line of symmetry direction and a point lying on that line is that the sum of the characters of the compatible representations should agree for the group of the wavevectors along that same line (Slater 1965). The symmetry vibration modes at individual points of phase I and II are also calculated by using the projection operator technique, and are listed in table 3 and table 5 below.

Previous investigations (Bulou *et al* 1983) showed the small dispersion of the phonon branches along Γ–Z (Z=(001)) and along the M–V–A direction for the ideal aristotype structure, which is consistent with the structure of the two-dimensional octahedral network. Further evidence of this characteristic layer structure is also obtained from our symmetry analyses. In table 1, despite the differences in wavevectors which resulted in different multipliers, the little groups at the M and A symmetry points of the aristotype structure are the same and the symmetry species of the modes that correspond to these two wavevectors have little difference. In addition, the symmetry vibration modes along M–V–A (the [001] axis) are essentially the same (table 3). The compatibility relations along the same direction (figure 3(*a*)) further indicate that the

Table 1. Symmetry properties of $RbAlF_4$ in phase I, space group P4/mmm (D_{4h}^1). The little group and the symmetry species corresponding to the individual wavevectors in the Brillouin zone are presented in Kovalev's notation (Kovalev 1965). The results from Bulou *et al* (1983) which applied Bradley's notation (Bradley and Cracknell 1972) are also listed in brackets for comparison. All the symmetry modes are singly degenerate except τ_9, τ_{10}, and τ_5 at the V point, which are doubly degenerate. The parameter $0.0 < \mu < 0.5$.

	k-vector	Little group	Symmetry species of the normal modes
Γ	(0,0,0)	T147	$\tau_1 + 4\tau_4 + \tau_8 + \tau_9 + 5\tau_{10}$ $(\Gamma_1^+ + 4\Gamma_2^- + \Gamma_4^- + \Gamma_5^+ + 5\Gamma_5^-)$
Δ	$(0, \mu, 0)$	T31	$6\tau_1 + \tau_2 + 6\tau_3 + 5\tau_4$
X	(0,0.5,0)	T32	$3\tau_1 + 3\tau_3 + 3\tau_4 + \tau_5 + 3\tau_6 + 2\tau_7 + 3\tau_8$
Y	$(\mu, 0.5, 0)$	T30	$6\tau_1 + 3\tau_2 + 4\tau_3 + 5\tau_4$
M	(0.5,0.5,0)	T147	$2\tau_1 + \tau_3 + 2\tau_4 + \tau_5 + \tau_6 + \tau_7 + 2\tau_9 + 3\tau_{10}$ $(2M_1^+ + M_2^+ + 2M_2^- + M_3^+ + M_3^- + M_4^+ + 2M_5^+ + 3M_5^-)$
V	$(0.5, 0.5, \mu)$	T119	$4\tau_1 + \tau_2 + \tau_3 + 2\tau_4 + 5\tau_5$
A	(0.5,0.5,0.5)	T147	$2\tau_1 + \tau_3 + 2\tau_4 + \tau_5 + 2\tau_7 + 3\tau_9 + 2\tau_{10}$

Table 2. Symmetry properties of $RbAlF_4$ in phase II, space group P4/mbm (D_{4h}^5). The little group and the symmetry species corresponding to the individual wavevectors in the Brillouin zone are presented in Kovalev's notation (Kovalev 1965). The results from Bulou *et al* (1983) which applied Bradley's notation (Bradley and Cracknell 1972) are also listed in brackets for comparison. All the symmetry modes are singly degenerate except τ_9, τ_{10}, and τ_1 and τ_2 at the X point, which are doubly degenerate. The parameter $0.0 < \mu < 0.5$.

	k-vector	Little group	Symmetry species of the normal modes
Γ	(0,0,0)	T147	$2\tau_1 + 2\tau_2 + 2\tau_3 + 4\tau_4 + \tau_5 + 2\tau_6 + \tau_7 + 3\tau_9 + 8\tau_{10}$ $(2\Gamma_1^+ + 2\Gamma_1^- + 2\Gamma_2^+ + 4\Gamma_2^- + \Gamma_3^+ + 2\Gamma_3^- + \Gamma_4^+ + 3\Gamma_5^+ + 8\Gamma_5^-)$
Δ	$(0, \mu, 0)$	T31	$11\tau_1 + 7\tau_2 + 7\tau_3 + 11\tau_4$
X	(0,0.5,0)	T61	$11\tau_1 + 7\tau_2$
Y	$(\mu, 0.5, 0)$	T58	$11\tau_1 + 11\tau_2 + 7\tau_3 + 7\tau_4$
M	(0.5,0.5,0)	T152	$3\tau_1 + 3\tau_2 + \tau_3 + 3\tau_4 + \tau_5 + 3\tau_6 + 3\tau_7 + 3\tau_8 + 5\tau_9 + 3\tau_{10}$ $(3M_1^- + 3M_4^+ + M_4^- + 3M_1^+ + M_3^- + 3M_2^+ + 3M_2^- + 3M_3^+ + 5M_5^- + 3M_5^+)$

vibration modes do not change their patterns in each phonon branch along M–V–A. The anisotropy of the compatibility along the [001] axis and along the [100] and [010] axes is also clearly shown in the same figure. The A_3–M_3 phonon branch, which is the τ_3–τ_2–τ_3 branch in figure 3(*a*) and corresponds to the tilts of the octahedra, is very flat (Bulou *et al* 1983). The τ_3 mode (M_2^+) at M is softened when the crystal approaches the transition temperature T_{c1}.

The normal vibration modes at the zone centre of phase I are calculated from the symmetry eigenvectors (table 3) by using further unitary transformation. They are presented in table 4. The fifteen non-acoustic phonon modes can be divided into five groups of vibration patterns each of which includes three orthogonal modes along [100], [010] and [001] separately. The two vibration modes in the (001) plane are doubly degenerate due to the characteristic layer structure. These vibration patterns

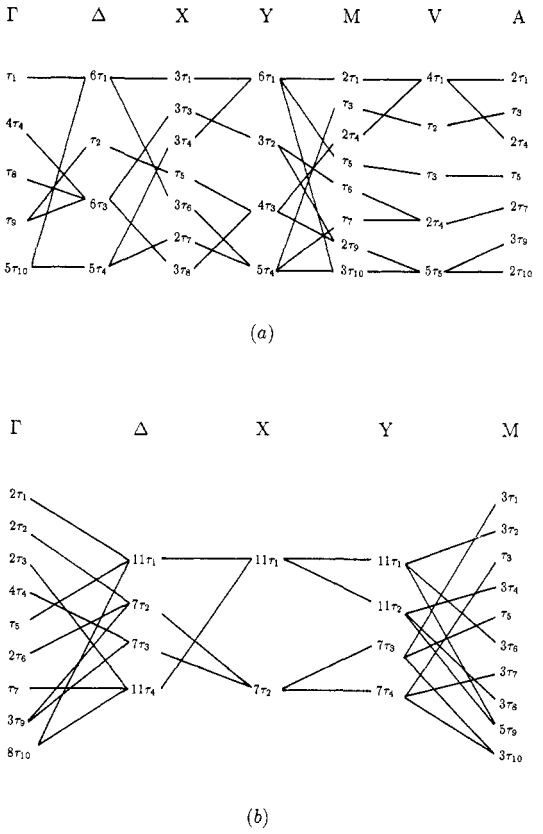

Figure 3. The compatibility relations along the symmetry direction Γ–Δ–X–Y–M–V–A in phase I (*a*) and along Γ–Δ–X–Y–M in phase II (*b*).

are illustrated in figure 4, and described in the following way.

(i) The τ_1 (A_{1g}) mode which involves the opposite displacements of the two F_{ax} ions, i.e. z_3–z_4, describes the stretching of the AlF_6 octahedra along the [001] direction, while the doubly degenerate mode τ_9 (E_g) corresponds to the sheer stretching of the AlF_6 octahedra in the (001) plane. τ_1 and τ_9 are Raman active modes with frequencies 543 cm^{-1} and 238 cm^{-1} respectively. The higher frequency of the τ_1 mode is consistent with the short Al–F_{ax} bond length (Bulou and Nouet 1982).

(ii) The bending of the F_{eq}–Al–F_{eq} bond along [001] is given by τ_8 (B_{2u}) and the bending of this bond in the equatorial plane is given by one of the doubly degenerate modes τ_{10} (E_u). These bendings consist of the opposite vibrations of the F_{eq} ions in three-dimensional space.

(iii) One of the τ_4 modes (A_{2u}) and another doubly degenerate mode τ_{10} (E_u) represent the distortion of the octahedra AlF_6, which is produced by the combination of bendings of the F_{eq}–Al–F_{eq} and F_{ax}–Al–F_{ax} bonds. They involve opposite vibrations of the F_{eq} and F_{ax} ions in the tetragonal lattice. The modes in group (ii) and (iii) are infrared modes. Their frequencies are in the range 500–160 cm^{-1} (Soga *et al* 1974).

(iv) The relative translational motion of the tetragonal lattice, including the Rb and Al ions, and the sublattice formed by the two-dimensional octahedral chain. The resultant motion of these vibrations is the asymmetric stretching of the F–Al bonds

Table 3. Symmetry vibration modes of $RbAlF_4$ in phase I, space group P4/mmm (D^1_{4h}).

Γ	Rb	Al	F_1, F_2 (F_{eq})	F_3, F_4 (F_{ax})	M	Rb	Al	F_1, F_2 (F_{eq})	F_3, F_4 (F_{ax})
τ_1				$z_3 - z_4$	τ_1			$x_1 + y_2$	$z_3 - z_4$
τ_4	z	z	$z_1 + z_2$	$z_3 + z_4$	τ_3			$y_1 - x_2$	
τ_8			$z_1 - z_2$		τ_4		z		$z_3 + z_4$
τ_9				$x_3 - x_4$	τ_5			$x_1 - y_2$	
				$y_3 - y_4$	τ_6	z			
τ_{10}	x	x	$x_1 + x_2$	$x_3 + x_4$	τ_7			$y_1 + x_2$	
			$x_1 - x_2$		τ_9			$z_1 + z_2$	$x_3 - x_4$
	y	y	$y_1 + y_2$	$y_3 + y_4$				$z_1 - z_2$	$y_3 - y_4$
			$y_1 - y_2$		τ_{10}	x	x		$x_3 + x_4$
						y	y		$y_3 + y_4$

V	Rb	Al	F_1, F_2 (F_{eq})	F_3, F_4 (F_{ax})	A	Rb	Al	F_1, F_2 (F_{eq})	F_3, F_4 (F_{ax})
τ_1		z	$x_1 + y_2$	$z_3 + z_4$	τ_1			$x_1 + y_2$	$z_3 - z_4$
				$z_3 - z_4$	τ_3			$y_1 - x_2$	
τ_2			$y_1 - x_2$		τ_4		z		$z_3 + z_4$
τ_3			$x_1 - y_2$		τ_5			$x_1 - y_2$	
τ_4	z		$y_1 + x_2$		τ_7	z		$y_1 + x_2$	
τ_5	x	x	$z_1 + z_2$	$x_3 + x_4$	τ_9	x		$z_1 + z_2$	$x_3 - x_4$
	y	y	$z_1 - z_2$	$x_3 - x_4$		y		$z_1 - z_2$	$y_3 - y_4$
				$y_3 + y_4$	τ_{10}		x		$x_3 + x_4$
				$y_3 - y_4$			y		$y_3 + y_4$

in three-dimensional space. These high-frequency infrared vibrations (800–500 cm^{-1}) include one of the τ_4 (A_{2u}) mode and one of the doubly degenerate modes τ_{10} (E_u) (Soga *et al* 1974).

(v) The last group of the vibration patterns is the relative translational motion of the sublattice of the Rb and Al ions. These are the low-frequency infrared modes with wavenumbers below 160 cm^{-1}. They include one of the τ_4 (A_{2u}) mode and one of the τ_{10} (E_u) modes.

The vibration patterns of the 36 symmetry modes in phase II at the zone centre (table 5) can be divided into four groups. The first group, which includes six eigenvectors $\tau_4+\tau_6+2\tau_{10}$, consists of the relative vibration and the translational motion of the two tetragonal sublattices formed by the Rb_1 and Rb_2 ions. Another six modes $\tau_2+\tau_4+2\tau_{10}$ describe the same kinds of motion for the Al_1 and Al_2 sublattices as those in the first group. The motions of the F_{eq} ions are given by 12 of the modes. Among them eight modes ($\tau_1+\tau_3+\tau_5+\tau_7+2\tau_{10}$) are in the equatorial plane, and four of them ($\tau_4+\tau_6+\tau_9$) are along the [001] axis. Four of the modes in the (001) plane, namely τ_1, τ_3, τ_5 and τ_7, describe the combination of stretching (squeezing) and tilting of the octahedra around the [001] axis, one of the τ_{10} modes represents the bending of the F_{eq}–Al–F_{eq} bonds in the equatorial plane, while another τ_{10} mode is the translational motion of the two dimensional octahedra chain in the (001) plane. These vibration patterns are illustrated in figure 5. It is the eigenvector τ_1 (A_{1g}) that here exhibits a soft mode behaviour as phase I is approached from a temperature below T_{c1} (Bulou *et al* 1983), and was assigned to the soft mode for the SPT at T_{c1}, which originates from the τ_3 zone boundary mode in the aristotype D^1_{4h} structure. The four modes $\tau_4+\tau_6+\tau_9$, which involve the vibrations along the [001] axis of the equatorial ions, are the translational

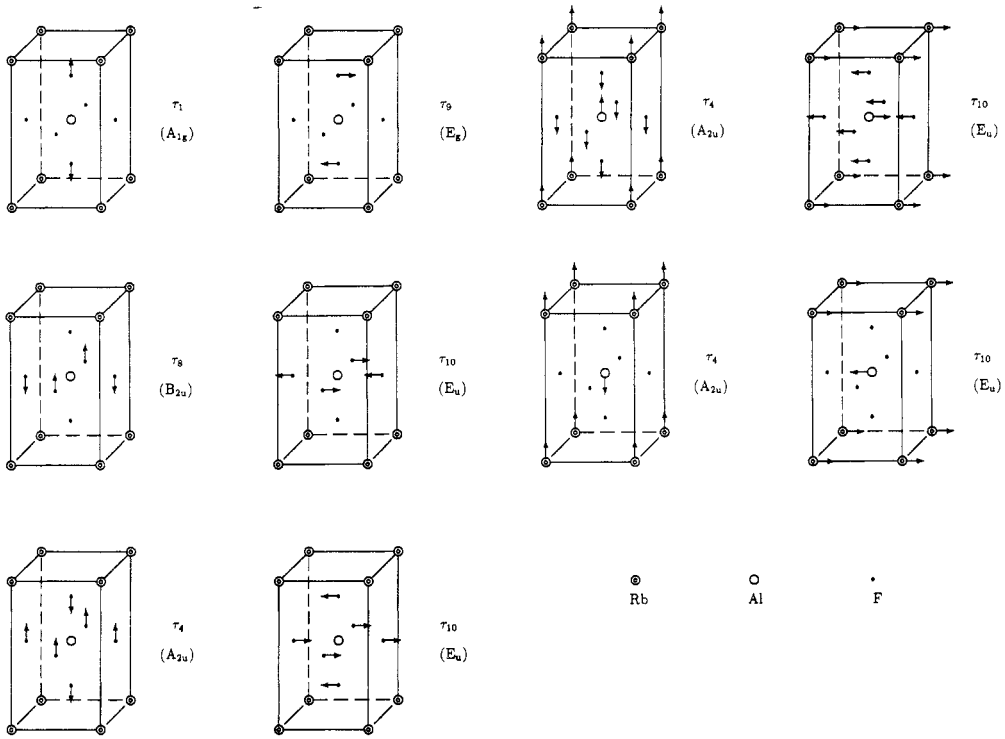

Figure 4. The normal vibration modes of $RbAlF_4$ in phase I at the zone centre Γ. Each of the doubly degenerate modes E_g and E_u consists of a pair of orthogonal vibrations along [010] and [100] separately. Only vibrations along [100] in each pair are presented.

Table 4. Normal vibration modes of $RbAlF_4$ in phase I at the zone centre Γ.

τ_1	(A_{1g})	$(1/\sqrt{2})(z_3 - z_4)$
τ_4	(A_{2u})	$(1/\sqrt{6})\ (z_{Rb} + z_{Al} + z_1 + z_2 + z_3 + z_4)$
		$(1/\sqrt{2})(z_{Rb} - z_{Al})$
		$(1/2)[(z_1 + z_2) - (z_3 + z_4)]$
		$(1/2\sqrt{3})[(2z_{Rb} + 2z_{Al}) - (z_1 + z_2) - (z_3 + z_4)]$
τ_8	(B_{2u})	$(1/\sqrt{2})(z_1 - z_2)$
τ_9	(E_g)	$(1/\sqrt{2})(x_3 - x_4)$
		$(1/\sqrt{2})(y_3 - y_4)$
τ_{10}	(E_u)	$(1/\sqrt{6})(x_{Rb} + x_{Al} + x_1 + x_2 + x_3 + x_4)$
		$(1/\sqrt{6})(y_{Rb} + y_{Al} + y_1 + y_2 + y_3 + y_4)$
		$(1/\sqrt{2})(x_{Rb} - x_{Al}),\quad (1/\sqrt{2})(y_{Rb} - y_{Al})$
		$(1/\sqrt{2})(x_1 - x_2),\quad (1/\sqrt{2})(y_1 - y_2)$
		$(1/2)[(x_1 + x_2) - (x_3 + x_4)],\quad (1/2)[(y_1 + y_2) - (y_3 + y_4)]$
		$(1/2\sqrt{3})[(2x_{Rb} + 2x_{Al}) - (x_1 + x_2) - (x_3 + x_4)]$
		$(1/2\sqrt{3})[(2y_{Rb} + 2y_{Al}) - (y_1 + y_2) - (y_3 + y_4)]$

(τ_4), the F_{eq}–Al–F_{eq} bond bending (τ_6), and the tilting of the octahedra around the [100] and [010] axes. The 12 eigenvectors for the F_{ax} ions can be discussed in a similar way.

Table 5. Symmetry vibration modes of $RbAlF_4$ in phase II, space group P4/mbm (D^5_{4h}). Here $p = (1 + i)$ and $m = (1 - i)$.

Γ	Rb_1, Rb_2	Al_1, Al_2	F_1, F_2, F_3, F_4 (F_{eq})	F_5, F_6, F_7, F_8 (F_{ax})
τ_1 (A_{1g})			$x_1 - y_1 + x_2 - y_2 - x_3 + y_3 - x_4 + y_4$	$z_5 - z_6 + z_7 - z_8$
τ_2 (A_{1u})		$z_1 - z_2$		$z_5 + z_6 - z_7 - z_8$
τ_3 (A_{2g})			$x_1 + y_1 - x_2 - y_2 - x_3 - y_3 + x_4 + y_4$	$z_5 - z_6 - z_7 + z_8$
τ_4 (A_{2u})	$z_1 + z_2$	$z_1 + z_2$	$z_1 + z_2 + z_3 + z_4$	$z_5 + z_6 + z_7 + z_8$
τ_5 (B_{1g})			$x_1 + y_1 + x_2 + y_2 - x_3 - y_3 - x_4 - y_4$	
τ_6 (B_{1u})	$z_1 - z_2$		$z_1 - z_2 + z_3 - z_4$	
τ_7 (B_{2g})			$x_1 - y_1 - x_2 + y_2 - x_3 + y_3 + x_4 - y_4$	
τ_9 (E_g)			$z_1 + z_2 - z_3 - z_4$	$x_5 + y_5 - x_6 - y_6 + x_7 + y_7 - x_8 - y_8$
			$z_1 - z_2 - z_3 + z_4$	$x_5 + y_5 - x_6 - y_6 - x_7 - y_7 + x_8 + y_8$
				$x_5 - y_5 - x_6 + y_6 + x_7 - y_7 - x_8 + y_8$
				$x_5 - y_5 - x_6 + y_6 - x_7 + y_7 + x_8 - y_8$
τ_{10}(E_u)	$x_1 + x_2$	$x_1 + x_2$	$x_1 + y_1 + x_2 + y_2 + x_3 + y_3 + x_4 + y_4$	$x_5 + y_5 + x_6 + y_6 + x_7 + y_7 + x_8 + y_8$
	$x_1 - x_2$	$x_1 - x_2$	$x_1 + y_1 - x_2 - y_2 + x_3 + y_3 - x_4 - y_4$	$x_5 + y_5 + x_6 + y_6 - x_7 - y_7 - x_8 - y_8$
	$y_1 + y_2$	$y_1 + y_2$	$x_1 - y_1 + x_2 - y_2 + x_3 - y_3 + x_4 - y_4$	$x_5 - y_5 + x_6 - y_6 + x_7 - y_7 + x_8 - y_8$
	$y_1 - y_2$	$y_1 - y_2$	$x_1 - y_1 - x_2 + y_2 + x_3 - y_3 - x_4 + y_4$	$x_5 - y_5 + x_6 - y_6 - x_7 + y_7 - x_8 + y_8$

M	Rb_1, Rb_2	Al_1, Al_2	F_1, F_2, F_3, F_4 (F_{eq})	F_5, F_6, F_7, F_8 (F_{ax})
τ_1	$pz_1 + mz_2$		$pz_1 + mz_2 - pz_3 - mz_4$	$px_5 + my_5 - px_6 - my_6$
				$-mx_7 - py_7 + mx_8 + py_8$
τ_2		$px_1 + my_1$	$mx_1 + my_1 + px_2 - py_2$	$px_5 + my_5 + px_6 + my_6$
		$+mx_2 + py_2$	$+mx_3 + my_3 + px_4 - py_4$	$+mx_7 + py_7 + mx_8 + py_8$
τ_3				$mx_5 - py_5 - mx_6 + py_6$
				$-px_7 + my_7 + px_8 - my_8$
τ_4		$px_1 + my_1$	$px_1 - py_1 + mx_2 + my_2$	$mx_5 - py_5 + mx_6 - py_6$
		$-mx_2 - py_2$	$+px_3 - py_3 + mx_4 + my_4$	$+px_7 - my_7 + px_8 - my_8$
τ_5				$px_5 - my_5 - px_6 + my_6$
				$-mx_7 + py_7 + mx_8 - py_8$
τ_6		$mx_1 + py_1$	$px_1 - py_1 - mx_2 - my_2$	$px_5 - my_5 + px_6 - my_6$
		$-px_2 - my_2$	$+px_3 - py_3 - mx_4 - my_4$	$+mx_7 - py_7 + mx_8 - py_8$
τ_7	$mz_1 + pz_2$		$mz_1 + pz_2 - mz_3 - pz_4$	$mx_5 + py_5 - mx_6 - py_6$
				$-px_7 - my_7 + px_8 + my_8$
τ_8		$mx_1 + py_1$	$mx_1 + my_1 - px_2 + py_2$	$mx_5 + py_5 + mx_6 + py_6$
		$+px_2 + my_2$	$+mx_3 + my_3 - px_4 + py_4$	$+px_7 + my_7 + px_8 + my_8$
τ_9	$x_1 + y_2$		$(x_1 + y_1) - (x_2 - y_2) - (x_3 + y_3) + (x_4 - y_4)$	$z_5 - z_6 + z_7 - z_8$
	$x_1 - y_2$		$(x_1 - y_1) + (x_2 + y_2) - (x_3 - y_3) - (x_4 + y_4)$	$z_5 - z_6 - z_7 + z_8$
	$y_1 + x_2$		$(x_1 + y_1) + (x_2 - y_2) - (x_3 + y_3) - (x_4 - y_4)$	
	$y_1 - x_2$		$(x_1 - y_1) - (x_2 + y_2) - (x_3 - y_3) + (x_4 + y_4)$	
τ_{10}		$z_1 + z_2$	$z_1 + z_2 + z_3 + z_4$	$z_5 + z_6 + z_7 + z_8$
		$z_1 - z_2$	$z_1 - z_2 + z_3 - z_4$	$z_5 + z_6 - z_7 - z_8$

3. Lattice dynamical interpretation into the SPT at T_{c1} and T_{c2}

The detailed structure of $RbAlF_4$ in its successive phases I, II and III, and the corresponding lattice parameters are given by Bulou and Nouet (1982). The tetragonal unit cell of phase I and II, and the orthorhombic unit cell of phase III are illustrated in figure 1. The unit cell parameters are related to each other as

$$a_{III} = \sqrt{2}a_{II} = 2a_I \qquad b_{III} = \sqrt{2}b_{II} = b_I \qquad c_{III} = c_{II} = c_I \qquad (a_I = b_I). \tag{1}$$

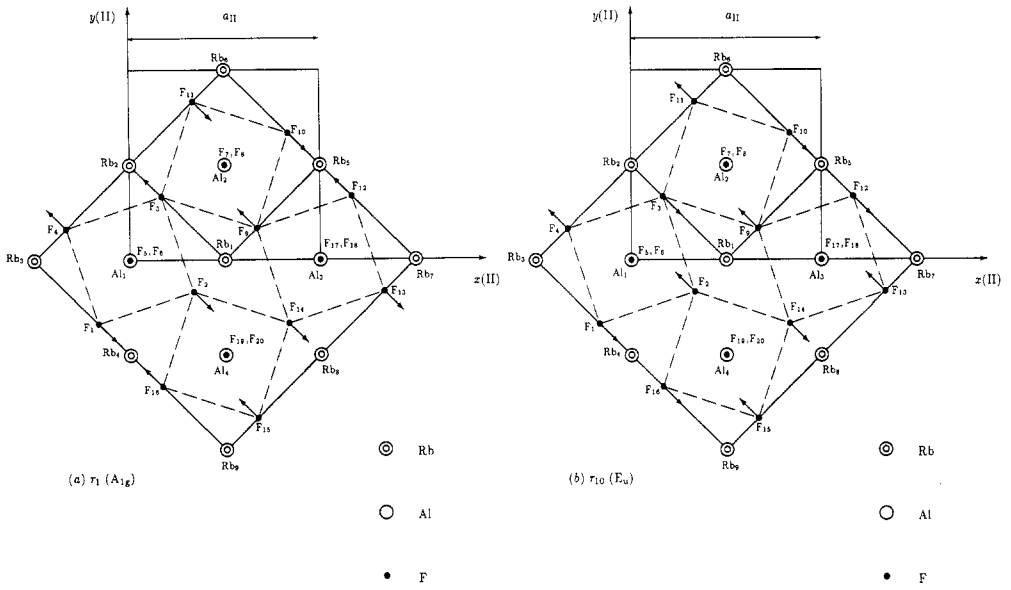

Figure 5. The symmetry vibration modes τ_1 (*a*) and τ_{10} (*b*) of $RbAlF_4$ in phase II at the zone centre Γ. They describe two different vibration patterns of the F_{eq} ions in the (001) plane.

The displacive non-ferroic phase transition at T_{c1} in $RbAlF_4$ is induced by the softening of the τ_3 (M_2^+) mode at the M point in the Brillouin zone. Our lattice mode analysis showed that the τ_3 mode at the wavevector $\boldsymbol{k} = (\frac{1}{2}\,\frac{1}{2}\,0)$ is $[y_1 - x_2]$ which involves only the motion of the F_{eq} atoms in the equatorial plane (table 1). As a result of the condensation of this mode, the atomic displacement $\boldsymbol{U}_{l\kappa}(\boldsymbol{r}_l)$, which describes the displacement of the κth atom in the lth unit cell from its equilibrium position, can be written as

$$\boldsymbol{U}_{l\kappa}(\boldsymbol{r}_l) = Q_{\boldsymbol{k}}\boldsymbol{e}_\kappa(\boldsymbol{k})\exp(\mathrm{i}\boldsymbol{k}\cdot\boldsymbol{r}_l). \tag{2}$$

Here $Q_{\boldsymbol{k}}$ is a complex normal mode coordinate, $\boldsymbol{e}_\kappa(\boldsymbol{k})$ is the eigenvector of the soft mode and $\boldsymbol{r}_l$ is the position vector of the atoms in the lth unit cell. For simplicity we assume that the phase of the complex coordinate $\Theta_{\boldsymbol{k}} = 0$. The calculated atomic displacement pattern of this soft mode gave exactly the tilting of the octahedra around the [001] axis which stimulated the displacive phase transition at T_{c1}.

The ferroelastic SPT at T_{c2} in $RbAlF_4$ is produced by two new tilts of the AlF_6 octahedra around the [010] and [100] axes, and the translational motions of the Rb ions along the [001] direction. These are associated with the softening of the complex conjugate modes τ_1 (M_1^-) and τ_7 (M_2^-) at the M point of the Brillouin zone. This ferroelastic phase transition can be interpreted in the following way. In phase II, the position vector $\boldsymbol{r}_{l\kappa}$ of the κth atom in the lth unit cell is given by

$$\boldsymbol{r}_{l\kappa} = \boldsymbol{r}^0_{l\kappa} + \boldsymbol{U}_{l\kappa}. \tag{3}$$

The vector $\boldsymbol{r}^0_{l\kappa}$ in equation (3) stands for the atomic equilibrium positions in the exact tetrahedral structure of phase II. These position vectors are listed in the first column of table 6. The vector $\boldsymbol{U}_{l\kappa}$ in equation (3) represents the displacements of the

Table 6. Atomic parameters for $RbAlF_4$. The first and the second column in this table present the equilibrium atomic positions $\boldsymbol{r}^0_{l\kappa}$ in phase II, referred to the tetrahedral (D^5_{4h}) and the orthorhombic (D^{13}_{2h}) unit cell respectively. The third column gives the $\boldsymbol{r}_{l\kappa}$ values at the a, b, c, d, e and f sites of the orthorhombic unit cell in phase III. The expected atomic displacements $\boldsymbol{U}_{l\kappa}$ during the phase transition at T_{c2} are listed in the last column. The parameters $x = 0.280$, $z = 0.277$, $\alpha = 0.022$, $\beta = 0.006$, $\gamma = 0.021$ and $\delta = 0.021$ are taken from Bulou and Nouet (1982).

	Phase II (D^5_{4h})	Phase II (D^{13}_{2h})	Phase III (D^{13}_{2h})	u_x, u_y, u_z
Rb_1	$\frac{1}{2}, 0, \frac{1}{2}$	$\frac{1}{2}, \frac{1}{2}, \frac{1}{2}$	$\frac{1}{2}, \frac{1}{2}, \frac{1}{2}+\delta$	$0, 0, \delta$
Rb_2	$0, \frac{1}{2}, \frac{1}{2}$	$\frac{1}{2}, 1, \frac{1}{2}$	$\frac{1}{2}, 1, \frac{1}{2}-\delta$	$0, 0, -\delta$
Rb_3	$-\frac{1}{2}, 0, \frac{1}{2}$	$0, 1, \frac{1}{2}$	$0, 1, \frac{1}{2}-\delta$	$0, 0, -\delta$
Rb_4	$0, -\frac{1}{2}, \frac{1}{2}$	$0, \frac{1}{2}, \frac{1}{2}$	$0, \frac{1}{2}, \frac{1}{2}+\delta$	$0, 0, \delta$
Rb_5	$1, \frac{1}{2}, \frac{1}{2}$	$1, \frac{1}{2}, \frac{1}{2}$	$1, \frac{1}{2}, \frac{1}{2}+\delta$	$0, 0, \delta$
Rb_6	$\frac{1}{2}, 1, \frac{1}{2}$	$1, 1, \frac{1}{2}$	$1, 1, \frac{1}{2}-\delta$	$0, 0, -\delta$
Rb_7	$\frac{3}{2}, 0, \frac{1}{2}$	$1, 0, \frac{1}{2}$	$1, 0, \frac{1}{2}-\delta$	$0, 0, -\delta$
Rb_8	$1, -\frac{1}{2}, \frac{1}{2}$	$\frac{1}{2}, 0, \frac{1}{2}$	$\frac{1}{2}, 0, \frac{1}{2}-\delta$	$0, 0, -\delta$
Rb_9	$\frac{1}{2}, -1, \frac{1}{2}$	$0, 0, \frac{1}{2}$	$0, 0, \frac{1}{2}-\delta$	$0, 0, -\delta$
Al_1	$0, 0, 0$	$\frac{1}{4}, \frac{3}{4}, 0$	$\frac{1}{4}, \frac{3}{4}, 0$	$0, 0, 0$
Al_2	$\frac{1}{2}, \frac{1}{2}, 0$	$\frac{3}{4}, \frac{3}{4}, 0$	$\frac{3}{4}, \frac{3}{4}, 0$	$0, 0, 0$
Al_3	$1, 0, 0$	$\frac{3}{4}, \frac{1}{4}, 0$	$\frac{3}{4}, \frac{1}{4}, 0$	$0, 0, 0$
Al_4	$\frac{1}{2}, -\frac{1}{2}, 0$	$\frac{1}{4}, \frac{1}{4}, 0$	$\frac{1}{4}, \frac{1}{4}, 0$	$0, 0, 0$
F_1	$x-\frac{1}{2}, -x, 0$	$0, 1-x, 0$	$0, 1-x, 0-\alpha$	$0, 0, -\alpha$
F_2	$x, x-\frac{1}{2}, 0$	$x, \frac{1}{2}, 0$	$x, \frac{1}{2}, 0-\alpha$	$0, 0, -\alpha$
F_3	$\frac{1}{2}-x, x, 0$	$\frac{1}{2}, \frac{1}{2}+x, 0$	$\frac{1}{2}, \frac{1}{2}+x, 0+\alpha$	$0, 0, \alpha$
F_4	$-x, \frac{1}{2}-x, 0$	$\frac{1}{2}-x, 1, 0$	$\frac{1}{2}-x, 1, 0+\alpha$	$0, 0, \alpha$
F_5	$0, 0, z$	$\frac{1}{4}, \frac{3}{4}, z$	$\frac{1}{4}+\beta, \frac{3}{4}-\gamma, z$	$\beta, -\gamma, 0$
F_6	$0, 0, -z$	$\frac{1}{4}, \frac{3}{4}, -z$	$\frac{1}{4}-\beta, \frac{3}{4}+\gamma, -z$	$-\beta, \gamma, 0$
F_7	$\frac{1}{2}, \frac{1}{2}, z$	$\frac{3}{4}, \frac{3}{4}, z$	$\frac{3}{4}-\beta, \frac{3}{4}-\gamma, z$	$-\beta, -\gamma, 0$
F_8	$\frac{1}{2}, \frac{1}{2}, -z$	$\frac{3}{4}, \frac{3}{4}, -z$	$\frac{3}{4}+\beta, \frac{3}{4}+\gamma, -z$	$\beta, \gamma, 0$
F_9	$1-x, \frac{1}{2}-x, 0$	$1-x, \frac{1}{2}, 0$	$1-x, \frac{1}{2}, 0-\alpha$	$0, 0, -\alpha$
F_{10}	$x+\frac{1}{2}, 1-x, 0$	$1, 1-x, 0$	$1, 1-x, , 0-\alpha$	$0, 0, -\alpha$
F_{11}	$x, x+\frac{1}{2}, 0$	$\frac{1}{2}+x, 1, 0$	$\frac{1}{2}+x, 1, 0+\alpha$	$0, 0, \alpha$
F_{12}	$\frac{3}{2}-x, x, 0$	$1, x, 0$	$1, x, 0-\alpha$	$0, 0, -\alpha$
F_{13}	$1+x, x-\frac{1}{2}, 0$	$\frac{1}{2}+x, 0, 0$	$\frac{1}{2}+x, 0, 0+\alpha$	$0, 0, \alpha$
F_{14}	$x+\frac{1}{2}, -x, 0$	$\frac{1}{2}, \frac{1}{2}-x, 0$	$\frac{1}{2}, \frac{1}{2}-x, 0+\alpha$	$0, 0, \alpha$
F_{15}	$1-x, -\frac{1}{2}-x, 0$	$\frac{1}{2}-x, 0, 0$	$\frac{1}{2}-x, 0, 0+\alpha$	$0, 0, \alpha$
F_{16}	$\frac{1}{2}-x, x-1, 0$	$0, x, 0$	$0, x, 0-\alpha$	$0, 0, -\alpha$
F_{17}	$1, 0, z$	$\frac{3}{4}, \frac{1}{4}, z$	$\frac{3}{4}-\beta, \frac{1}{4}+\gamma, z$	$-\beta, \gamma, 0$
F_{18}	$1, 0, -z$	$\frac{3}{4}, \frac{1}{4}, -z$	$\frac{3}{4}+\beta, \frac{1}{4}-\gamma, -z$	$\beta, -\gamma, 0$
F_{19}	$\frac{1}{2}, -\frac{1}{2}, z$	$\frac{1}{4}, \frac{1}{4}, z$	$\frac{1}{4}+\beta, \frac{1}{4}+\gamma, z$	$\beta, \gamma, 0$
F_{20}	$\frac{1}{2}, -\frac{1}{2}, -z$	$\frac{1}{4}, \frac{1}{4}, -z$	$\frac{1}{4}-\beta, \frac{1}{4}-\gamma, -z$	$-\beta, -\gamma, 0$

individual atoms as a result of the condensation of the phonon modes τ_1 and τ_7 at T_{c2}. The equilibrium position vectors $\boldsymbol{r}^0_{l\kappa}$ of the atoms in phase II are transformed into the corresponding orthorhombic unit cell of phase III using the relationships

$$\begin{aligned} x_{III} &= \tfrac{1}{2}x_{II} + \tfrac{1}{2}y_{II} + \tfrac{1}{4} \\ y_{III} &= -\tfrac{1}{2}x_{II} + \tfrac{1}{2}y_{II} + \tfrac{3}{4} \\ z_{III} &= z_{II}. \end{aligned} \tag{4}$$

These orthorhombic positions for the atoms in phase II are also listed in the second column of table 6. The third column of table 6 gives the (a), (b), (c), (e), (f) and (g) sites of the orthorhombic unit cell (Pmmn, D_{2h}^{13}) which should be occupied by the atoms under equilibrium in phase III. These sites are represented by $\boldsymbol{r}_{l\kappa}$ in equation (3). During the SPT at T_{c2}, the condensation of the complex conjugate modes τ_1 and τ_7 at $\boldsymbol{k} = (\frac{1}{2}\ \frac{1}{2}\ 0)$ will provide the neccesary displacements $\boldsymbol{U}_{l\kappa}$ for each atom to move from its regular positions $\boldsymbol{r}_{l\kappa}^0$ in phase II (table 6, column 2) to its new equilibrium position $\boldsymbol{r}_{l\kappa}$ in phase III (table 6, column 3). These displacements are predicted by comparing column 2 and column 3 in table 6, and are listed in column 4 in the same table.

By using suitable linear combinations of the τ_1 and τ_7 modes derived from our normal vibration analysis (table 5), we are able to further calculate these expected displacements. The displacements of the atoms due to the condensation of the two complex conjugate modes at $\boldsymbol{k} = (\frac{1}{2}\ \frac{1}{2}\ 0)$ can be written as

$$\boldsymbol{U}_{l\kappa}(\boldsymbol{r}_l^0) = Q_1 \boldsymbol{e}_{1\kappa}(\boldsymbol{k}) \exp(\mathrm{i}\boldsymbol{k}\cdot\boldsymbol{r}_l^0) + Q_2 \boldsymbol{e}_{7\kappa}(\boldsymbol{k}) \exp(\mathrm{i}\boldsymbol{k}\cdot\boldsymbol{r}_l^0). \tag{5}$$

From table 5, the expected displacements of the Rb ions along the [001] axis are obtained by letting $Q_1 = -Q_2 = -\mathrm{i}$. Thus, we have

$$(-\mathrm{i})[(1+\mathrm{i})z_1 + (1-\mathrm{i})z_2] + (\mathrm{i})[(1-\mathrm{i})z_1 + (1+\mathrm{i})z_2] = 2z_1 - 2z_2 \tag{6}$$

which agree with those predicted in table 6. Similarly, the neccesary displacements of the F_{eq} ions are also correctly given by choosing $Q_1 = Q_2 = -1$.

$$\begin{aligned}(-1)[(1+\mathrm{i})z_1 + (1-\mathrm{i})z_2 - (1+\mathrm{i})z_3 - (1-\mathrm{i})z_4] + (-1)[(1-\mathrm{i})z_1 + (1+\mathrm{i})z_2 - (1-\mathrm{i})z_3 - (1+\mathrm{i})z_4] \\ = -2z_1 - 2z_2 + 2z_3 + 2z_4.\end{aligned} \tag{7}$$

The displacements of other atoms which are not in the same unit cell can be calculated in the same way by considering the corresponding position vectors $\boldsymbol{r}_l^0$ in equation (5). The results are in overall agreement with the expectation from column 4 of table 6. There are no dynamical displacements for the Al ions during the phase transformation. The transition displacements of the F_{ax} ions are given similarly by assuming $Q_1 \neq Q_2$ and with opposite phases. Thus, we have

$$\begin{aligned}&Q_1[(1+\mathrm{i})x_5 + (1-\mathrm{i})y_5 - (1+\mathrm{i})x_6 - (1-\mathrm{i})y_6 - (1-\mathrm{i})x_7 - (1+\mathrm{i})y_7 + (1-\mathrm{i})x_8 + (1+\mathrm{i})y_8] \\ &-Q_2[(1-\mathrm{i})x_5 + (1+\mathrm{i})y_5 - (1-\mathrm{i})x_6 - (1+\mathrm{i})y_6 - (1+\mathrm{i})x_7 - (1-\mathrm{i})y_7 + (1+\mathrm{i})x_8 + (1-\mathrm{i})y_8].\end{aligned} \tag{8}$$

Remembering that the coordinates in the tetragonal unit cell of phase II should be transformed into the orthorhombic unit cell by using equation (4), we derived

$$\begin{aligned}\delta x_5 &= (Q_1 - Q_2) & \delta x_6 &= -(Q_1 - Q_2) \\ \delta x_7 &= -(Q_1 - Q_2) & \delta x_8 &= (Q_1 - Q_2) \\ \delta y_5 &= (-\mathrm{i})(Q_1 + Q_2) & \delta y_6 &= (\mathrm{i})(Q_1 + Q_2) \\ \delta y_7 &= (-\mathrm{i})(Q_1 + Q_2) & \delta y_8 &= (\mathrm{i})(Q_1 + Q_2).\end{aligned} \tag{9}$$

Choosing properly the values for Q_1 and Q_2, we can eventually obtain the exact displacement magnitudes for the F_{ax} ions predicted by column 4 in table 6. Since

$(Q_1 + Q_2) = \gamma > (Q_1 - Q_2) = \beta$, the change of the crystal symmetry from tetrahedral to orthorhombic ($a_{III} \simeq b_{III}$ and $a_{III} \neq b_{III}$) at T_{c2} could be explained by the asymmetric displacements of the F_{ax} ions arising from the soft phonon modes during the phase transition. The above interpretation of the successive displacive phase transitions at T_{c1} and T_{c2} from our symmetry and lattice vibration study is in good agreement with the result from the experimental investigation (Bulou *et al* 1983, 1987).

It should be mentioned that there are some additional features in the Raman spectrum of $RbAlF_4$ that cannot be explained by the $q = 0$ selection rules. They are the result of a possible structure order–disorder occuring in phase I and II, and probably involve only the fluorine ions in the layers of octahedra (Bulou *et al* 1983). This hypothesis is supported by the observation of diffuse x-ray scattering and of a modulated background in neutron diffraction patterns (Mokhlisse *et al* 1983). Although we did not take this possible order–disorder feature and the non-rigidity of the AlF_6 octrahedra into our consideration, the interpretation of the phase transition in $RbAlF_4$ from our lattice dynamical study is still encouraging.

References

Brosset C 1937 *Z. Anorg. Allg. Chem.* **235** 139

Bradley C J and Cracknell A P 1972 *The Mathematical Theory of Symmetry in Solids* (Oxford: Clarendon)

Bulou A, Launay J M, Rosseau M, Ridon C and Nouet J 1984 *Ferroelectrics* **54** 249

Bulou A and Nouet J 1982 *J. Phys. C: Solid State Phys.* **15** 183

Bulou A, Rosseau M and Nouet J 1987 *Phase Transitions* **9** 139

Bulou A, Rosseau M, Nouet J, Loyzance P L, Mokhlisse R and Couzi M 1983 *J. Phys. C: Solid State Phys.* **16** 4527

Kleemann W, Schafer F J and Nouet J 1982 *J. Phys. C: Solid State Phys.* **15** 197

Kovalev O V 1965 *Irreducible Representations of the Space Group* (Gordon and Breach: New York)

Maradudin A A and Vosko S H 1968 *Rev. Mod. Phys.* **40** 1

Mokhlisse R, Couzi M and Loyzance P L 1983 *J. Phys. C: Solid State Phys.* **16** 1353, 1367

Rosseau M 1979 *J. Physique Lett.* **40** 439

Slater J C 1965 *Quantum Theory of Molecular Solids* (McGraw-Hill: New York)

Soga T, Ohwada K and Iwasaki M 1974 *J. Chem. Phys.* **61** 1990